Hindawi
Journal of Spectroscopy
Volume 2022, Article ID 8422803, 9 pages
https://doi.org/10.1155/2022/8422803

Research Article

Characterization and Optical Studies of Hydroxyethyl Cellulose-Copper Oxide Nanocomposites

A. S. A. Alsubaie

Department of Physics, College of Khurma University College, Taif University, P.O. Box 11099, Taif 21944, Saudi Arabia

Correspondence should be addressed to A. S. A. Alsubaie; asubaie@tu.edu.sa

Received 8 April 2022; Revised 31 May 2022; Accepted 14 June 2022; Published 8 July 2022

Academic Editor: Dong Lu

In this study, monometallic copper oxide nanoparticles (CuONPs) were synthesized by chemical reduction of copper sulfate ($CuSO_4$) salt through sugar glucose. X-ray diffraction profiles approved the formation of metallic oxide nanoparticles. TEM images showed spherical nanoparticles with an average particle size of 60 nm. The interaction of HEC and copper oxide nanoparticles was investigated by FTIR spectroscopy. The UV-visible absorption spectrum showed a surface plasmon resonance peak at 270 nm. The effect of doping of copper oxide nanoparticles (CuONPs) on the optical and thermal properties of HEC was studied. The results showed that the concentration of CuO nanoparticles has a prominent influence on the optical, structural, and thermal properties of hydroxyethyl cellulose.

1. Introduction

Polymeric nanocomposites are one of the interesting materials in the plastic industry. They attracted the attention of the researcher because of their high performance. Polymeric nanocomposites usually have a polymer or copolymer with nanoparticles or nanofiber dispersed in the polymer matrix. They combine the advantage of both polymers and metal nanoparticles [1]. Metal nanoparticles have distinctive and incredible electrical, optical, and thermal properties [2–4] while the polymer matrices have long time stability [5, 6]. Polymeric nanocomposites have different potential applications such as nanoelectronic devices, optical devices, optoelectronic, and sensors [7–9].

The hydroxyethyl cellulose (HEC) polymer is relatively cheap and has many applications in industry. It is largely used as a water-binder and thickening agent, stabilizer in many industrial applications [10].

Copper oxide nanoparticles (CuONPs) have drawn attention mostly because of their unique optical and electrical, thermal, and magnetic properties [11]. Copper oxide is a p-type semiconductor metal with a narrow band gap. It was used in several applications, such as gas sensors, the development of supercapacitors, catalysis, near-infrared filters, magnetic storage media, solar energy conversion, and field emission emitters [12]. The fluid viscosity and thermal conductivity of nanofluids can be improved and enhanced by including CuO nanoparticles [13]. It also has many applications in nanomedicine and biomedical sciences [14].

Different methods such as thermal decompositions of metallic precursors, photo- or chemical reduction of metal ions in an aqueous medium with various polymer surfactants, chemical vapor deposition, coprecipitation, impregnation, and microwave irradiation can be used for the preparation of metallic nanoparticles. The green chemistry methods are eco-friendly synthetic methods for the synthesis of nanomaterials. It has several advantages such as simplicity, cheap cost, compatibility for catalysis, and biomedical and pharmaceutical fields as well as for large-scale commercial applications [15–17].

In this work, the concentration impact of the copper oxide nanoparticle content in HEC on the optical and thermal characterization of hydroxyethyl cellulose will be investigated as well as the support morphological analysis.

2. Experimental

2.1. Samples Preparation. Hydroxyethyl cellulose (HEC) was purchased from Sigma-Aldrich Company. The average molecular weight and viscosity of HEC are approximately 250000 and 80–125 MPa. respectively. Copper sulfate

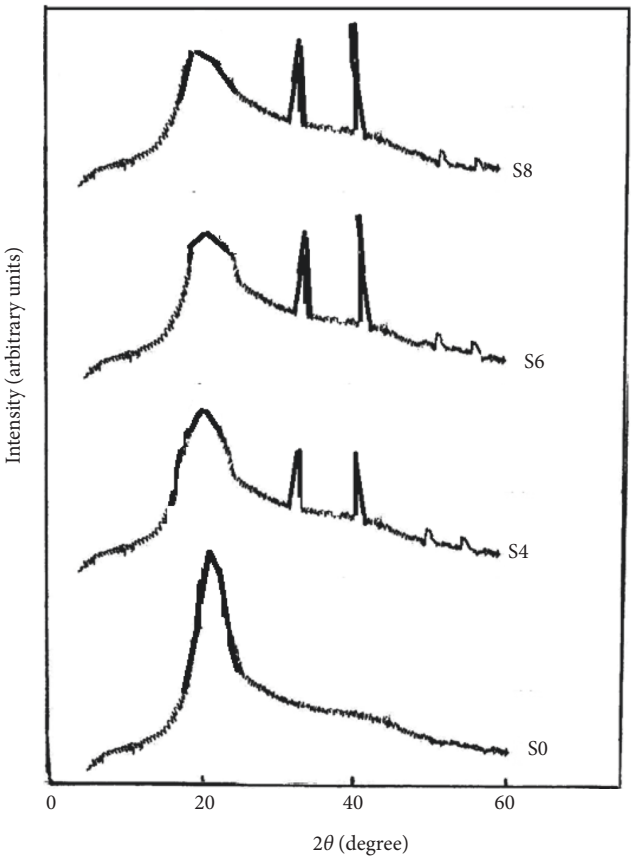

Figure 1: X-ray diffraction profiles of CuONPs-doped HEC samples.

($CuSO_4$) and glucose were analytic grade reagents and were supplied by Wako Chemicals Industries. Sodium hydroxide (NaOH) (Merck) was used as received. Colloidal copper solutions were prepared according to Panigrah et al. [12, 18, 19]. Two grams of glucose were dissolved in 25.0 mL of double-distilled water, and then, 150 μL of 0.1 M sodium hydroxide was added to the solution and the last mixture was heated to 50°C. Then, 1.0 mL of 0.01 M anhydrous copper sulfate solution was added to the hot mixture and heated until yellow color appeared. HEC was dissolved in double-distilled water by magnetic stirring at room temperature. Solutions of CuONPs and HEC have been mixed together to give 4, 6, and 8 wt.% of CuONPs-doped HEC using a magnetic stirrer at 50°C. A pure HEC sample is indicated as S0 while CuONPs-doped HEC samples were indicated as Sx, where x is the CuONPs wt.%. The nanocomposite was cast in a stainless steel Petri dish and then left to dry in the open air at room temperature (25°C) for four days until the solvent was completely evaporated. Films of the nanocomposite of the thickness of ~50 μm were formed.

2.2. Spectroscopic and Thermal Measurements. X-ray diffraction measurements of the film were performed using a Bruker AXS D8 Discover diffractometer with GADDS (general area detector diffraction system) operating with a Cu-Kα radiation source filtered with a graphite monochromator ($\lambda = 1.5406$ Å). The morphology and size of the CuO nanoparticles were examined by Joel transmission electron microscopy (TEM) (JEM-1011) which operates at 80 kV. The UV-vis absorption measurements were made using a spectrophotometer (Perkin-Elmer lambda 4β) throughout the wavelength range of 190–1000 nm. The FTIR spectra were collected in the range of 4000–400 cm^{-1} using a PYE spectrophotometer. The thermal analysis of the samples (TG/DTG/DTA) was performed using a Schimadzu DTG-60H thermal analyzer. Around three milligrams of nanocomposite material were put in a platinum crucible. The measurements were made in the presence of α-Al_2O_3 as a reference. The temperature increased from room temperature (25°C) to 1000°C at a ramp rate of 10°C/min. The TG/DTG/DTA measurements were performed in nitrogen gas flow with a flow rate of 20 ml/min.

3. Results and Discussion

3.1. X-Ray Diffraction. Figure 1 shows the X-ray diffraction profiles of CuONPs-doped HEC films at room temperature in the scanning range $6^\circ \le 2\theta \le 60^\circ$. The spectrum of HEC film exhibits an amorphous halo with scattered intensity maximum centered at $2\theta = 22^\circ$, and this is an indication of the amorphous nature of the undoped polymer. For doped HEC films, diffraction peaks appeared approximately at $2\theta = 35^\circ$, 39°, 49°, and 58° with varying intensities which give and evidence of the formation of CuONPs within the polymer matrix [20]. It is seen that the diffraction peak at $2\theta = 22^\circ$ that corresponds to the HEC film is shifted to lower angles with lower intensity and increasing broadening with increasing the CuONPs content. This behavior is an indication of the chemical interactions between HEC and CuONPs [21].

3.2. TEM and FTIR Measurements. TEM analysis showed that the colloidal solution of CuO nanoparticles has spherical nanoparticles of the average size of 60 nm as shown in Figure 2(a). The obtained particle size was in good agreement with previous studies [22, 23].

Figure 2(b) showed the TEM micrograph of the 8 wt% CuONPs-HEC composite sample. The TEM analysis showed that the CuO nanoparticles are highly dispersed in hydroxyethyl cellulose. The particle size of CuO increased to a diameter of ≈78 nm. The polymer prevented the agglomeration of CuO nanoparticles because due to the binder functions of the polymer [24]. Hydroxyethyl cellulose limits the motion of the synthesized nanoparticles. The FTIR spectroscopy measurements were performed to investigate the electrostatic interactions between HEC and CuO nanoparticles. Figure 3 shows the infrared spectra of HEC doped with CuO nanoparticles. For pure HEC(S0 sample) [25], the abroad band occurs in the range 3000–3600 cm^{-1} and this might be referred to as stretching vibration of H-bonded OH groups. The bands that appeared at 2910 and 2844 $cm^{-1}$are attributed to asymmetric and symmetric vibration of CH_2 groups, respectively. O-H deformation vibrations were observed at 1385 cm^{-1} [25].

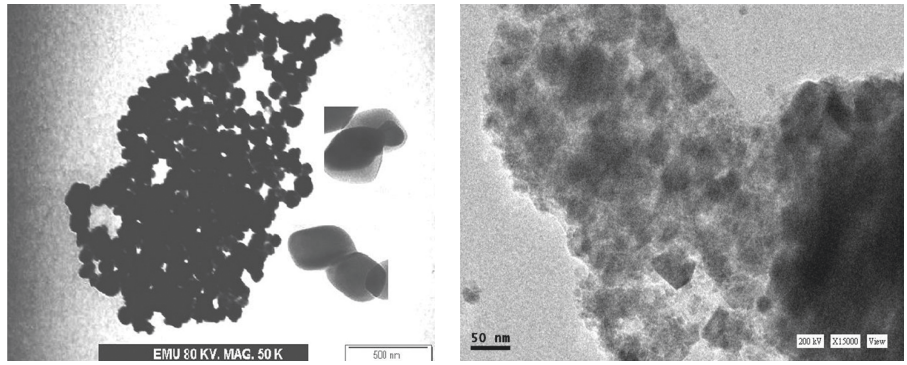

(a) (b)

Figure 2: TEM image of the (a) CuO colloids and (b) 8 wt% CuONPs-doped HEC sample.

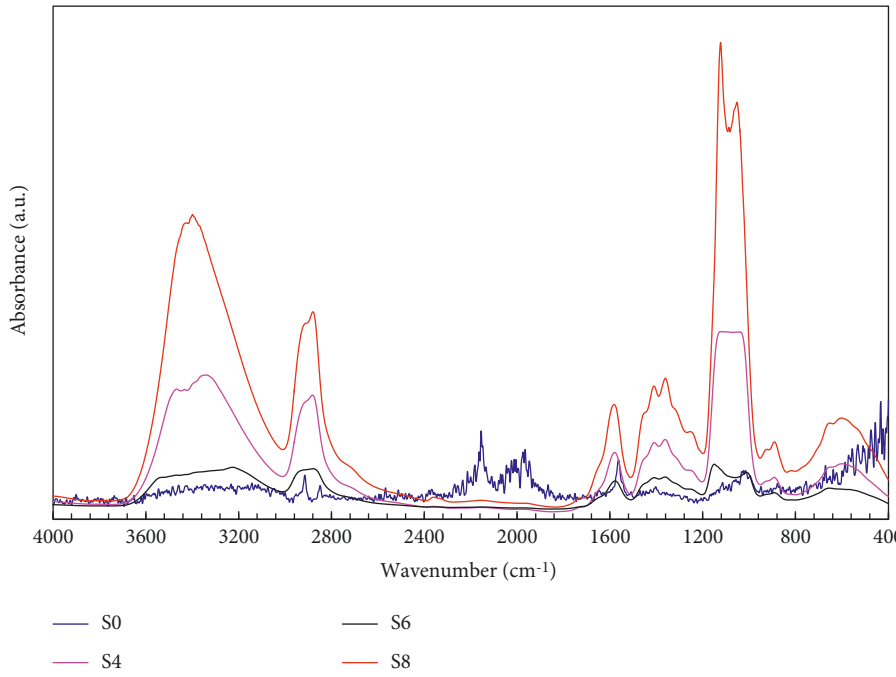

Figure 3: FTIR spectra of CuONPs-doped HEC samples.

The band at 1560 cm^{-1} indicates symmetric vibration C=O groups in the polymer. The band at 1399 cm^{-1} is designated to C-H deformation, and the bands at 1011 and 1111 are attributed to stretching C-OH vibrations. The small intensity bans at 896 cm^{-1} are attributed to β-glucoside linkage [26–28].

It is observed that with the addition of CuONPs to HEC, the intensity of bands that appeared in the range 3000–3600 cm^{-1} is increased which characterizes similar modes of vibrations of O-H [25]. The bands at 2844 and 2910 cm^{-1} overlabed with increasing intensity and bands at 2152 and 1963 cm^{-1} disappeared. The carbonyl group band at 1560 cm^{-1} is shifted toward 1596 cm^{-1}, and this indicates the oxidation of hydroxyl groups of the polymer and more formation of C=O groups. The bands in the range from 1418 to 898 cm^{-1} have a small shift to a higher frequency with increasing intensity. A new band appeared at 630 cm^{-1}, and this was assigned to ν_δ(OH). From the above discussion of IR spectra, it can be concluded that there is a strong electrostatic interaction between CuO nanoparticles and hydroxyethyl cellulose polymer.

3.3. Thermal Analysis

3.3.1. Differential Thermal Analysis (DTA). The differential thermal analysis (DTA) is a dynamic technique that can give valuable information about polymorphic phase transitions, melting, chemical reactions, and crystallization. The DTA thermograms of CuONPs-doped HEC films that started from room temperature up to 1000 C are shown in Figure 4. The various phase transitions are listed in Table 1. Sample S0 (pure HEC) shows two different endothermic phase transitions at 70

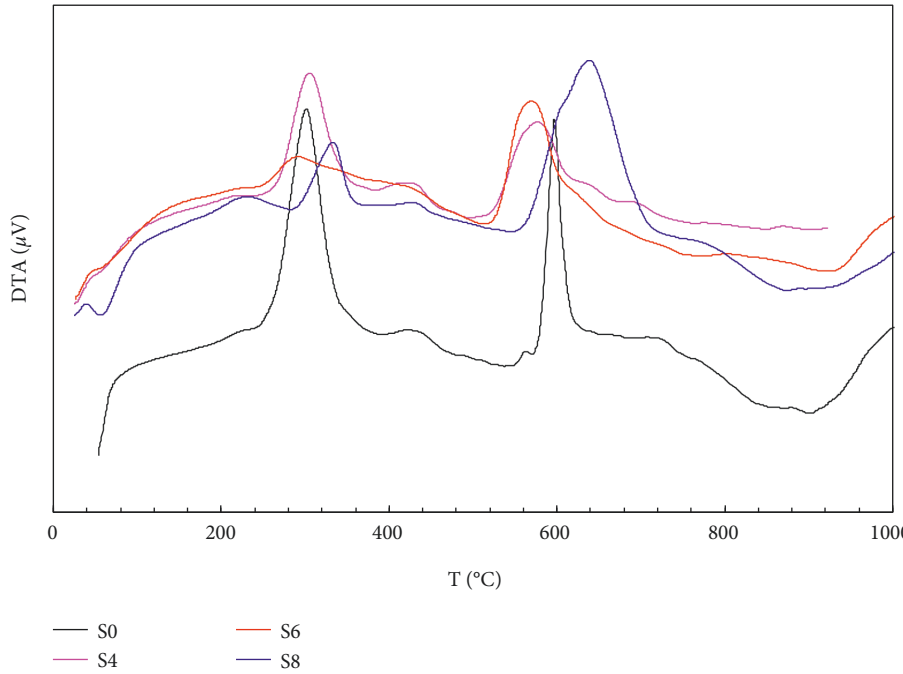

Figure 4: DTA curves of CuONPs-doped HEC samples.

Table 1: Transition temperatures for CuONPs-doped HEC samples.

Sample	Glass phase transition	Melting phase transition (T_m)	New phase transitions	
	T_g°C	T_m°C	*T_{p1}°C	**T_{p2}°C
S0	70	320	305 599	243
S4	55	322	310 432 585	516
S6	54	324	295 574	514
S8	50	345	338 643	289

and 320°C, and they are assigned to glass and melting phase transitions, respectively. This result showed good agreement with previous report results [29].

The observed endothermic peak at 243°C might attribute to the α-relaxation correlated with the crystalline areas while the exothermic peaks appearing at temperatures of 305 and 599°C are assigned to different degradation processes that occur in HEC [30]. By loading copper oxide nanoparticles into the pure polymer, it was noted a decrease in glass transition temperature. This is might happen because the segmental motion of HEC polymer amorphous becomes less inflexible [31]. Furthermore, it was noticed that the melting temperatures increased after loading CuO nanoparticles. The increment of melting temperature might refer to the increase in the molecular weight of HEC. Moreover, the high inner microstructure transition or high inter- and intramolecular hydrogen bonding might also increase the melting temperature [32]. Also, different endo and exothermic transitions appeared after mixing polymer and copper nanoparticles. The structural modification of HEC with CuONPs was indicated by the phase transitions and temperature changes.

3.3.2. Thermogravimetry (TGA) and Differential Thermogravimetry (DrTGA). Figure 5 shows the TGA and DrTGA thermograms of CuONPs-doped HEC system heated in a nitrogen atmosphere. It was noted from the figure that the thermal degradation of HEC-doped copper oxide nanoparticles film exhibit three weight loss stages.

As seen in Table 2, the weight loss starts in the range of 26–126°C with weight loss of about 1.75–11.79%. This is due to the evaporatization of the trapped water and/or the loss of adsorbed moisture. The second stage takes place at 170–480°C with weight loss of about 59.44–61.25% implying

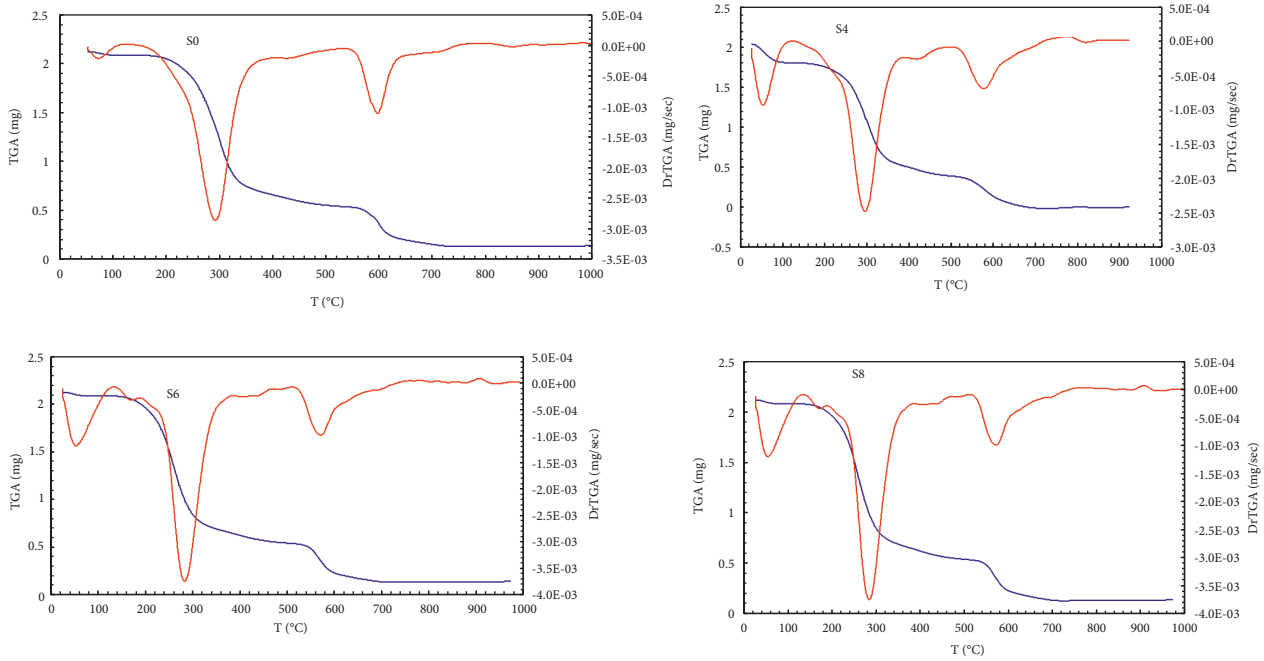

Figure 5: TGA and DrTGA curves of CuONPs-doped HEC samples.

Table 2: TG and DrTG data for CuONPs-doped HEC samples.

Sample	Region of decomposition	Temperature°C			%Weight loss	
		Start	End	T*p	Partial	Total
S0	1st	26	101	80	1.75	91.04
	2nd	170	351	298	61.25	
	3rd	351	725	601	28.04	
S4	1st	26	102	60	10.10	89.13
	2nd	102	458	299	60.36	
	3rd	458	707	585	18.67	
S6	1st	26	118	58	12.09	87.24
	2nd	118	484	288	59.01	
	3rd	484	802	578	16.14	
S8	1st	26	126	60	11.79	91.10
	2nd	126	480	289	59.44	
	3rd	480	708	577	19.87	

the removal reactions of water and residual acetate groups. These are probably due to the partially hydrolyzed form of HEC. The final degradation step occurs between 351 and 60°C with weight loss of 16.14–28.04%. The final degradation step is more sophisticated and involves polyene residue degradation to produce metallic residues and hydrocarbons [33].

It was observed that the loading of copper oxide nanoparticles has no significant impact on the thermal stability of hydroxyethyl cellulose. As a whole, no significant changes have been noted in the thermal stability of all composite samples.

3.4. Optical Properties

3.4.1. Optical Absorbance Spectra. Figure 6 shows the optical absorbance spectra of copper nanoparticles-doped hydroxyethyl cellulose samples. The spectra of HEC exhibited a hump at 206 nm which may be attributed to $n-\pi^*$ electronic transitions [34, 35].

It is observed that as the content of CuONPs increases the optical absorbance increases in the full-wavelength range. The UV-visible spectrum of HEC-doped CuO samples showed a red shift of 8 nm for the position of the hump. This red shift can be attributed to the variation of crystallinity of the doped polymer [32]. Also, a shoulder-like band is observed at 270 nm which has been attributed to the characteristic peak of CuONPs [36].

3.5. Optical Parameters. Equation (1) was used to calculate the absorption coefficient, $\alpha(\nu)$, as well as each curve near the edges [37]:

$$\alpha(\nu) = \frac{-1}{d}\ln\left[\frac{-(1-R)^2}{2TR^2} + \sqrt{\frac{(1-R)^4}{4T^2R^4} + \frac{1}{R^2}}\right], \quad (1)$$

where d is the thickness of the film sample; R is the reflectance; T is the transmittance of the sample for the incident photon.

The shift observed in the fundamental absorption edge of UV-visible spectra can be correlated with the optical band gap by Tauc's expression [34]:

$$\alpha(\nu)h\nu = B\left(h\nu - E_{opt}\right)^n, \quad (2)$$

where E_{opt} is the optical band gap energy; B is a constant called band tailing parameter; ν is the frequency; n is the index that can have different values $n = 1/3$, ½, 3, and 2 depending on the mechanism of interband transitions that is corresponding to direct forbidden transitions, direct

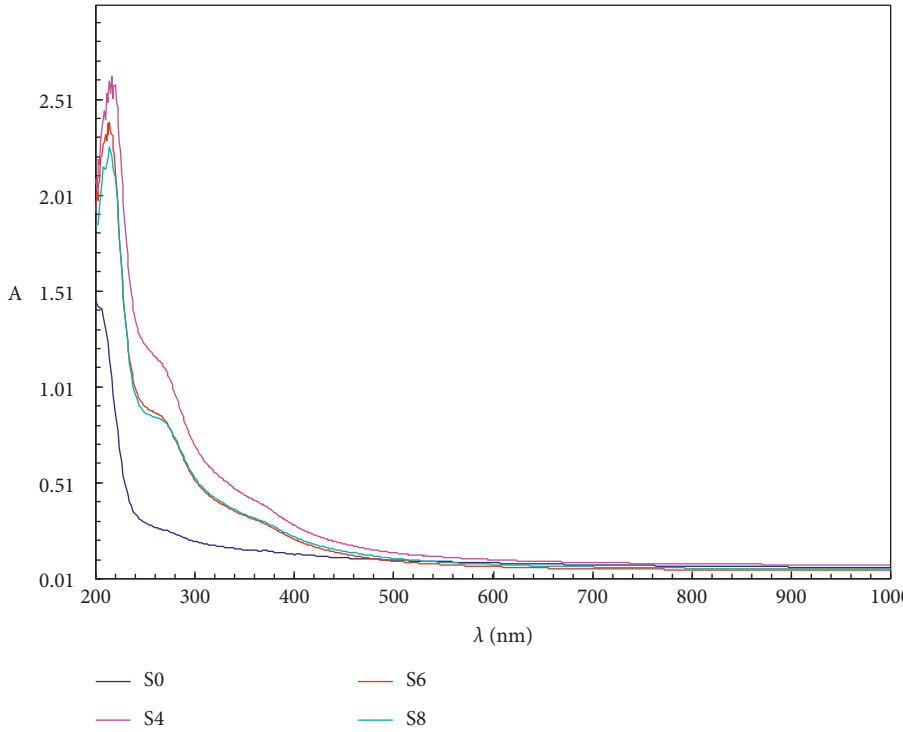

Figure 6: UV-visible spectra of CuONPs-doped HEC samples.

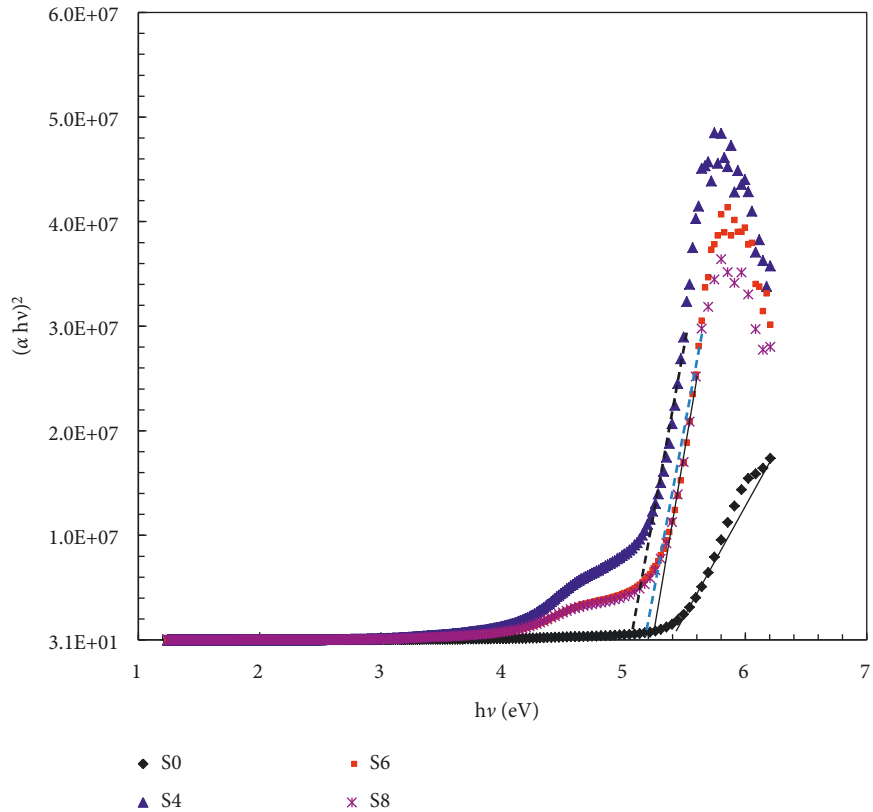

Figure 7: Tauc's plot of CuONPs-doped HEC samples.

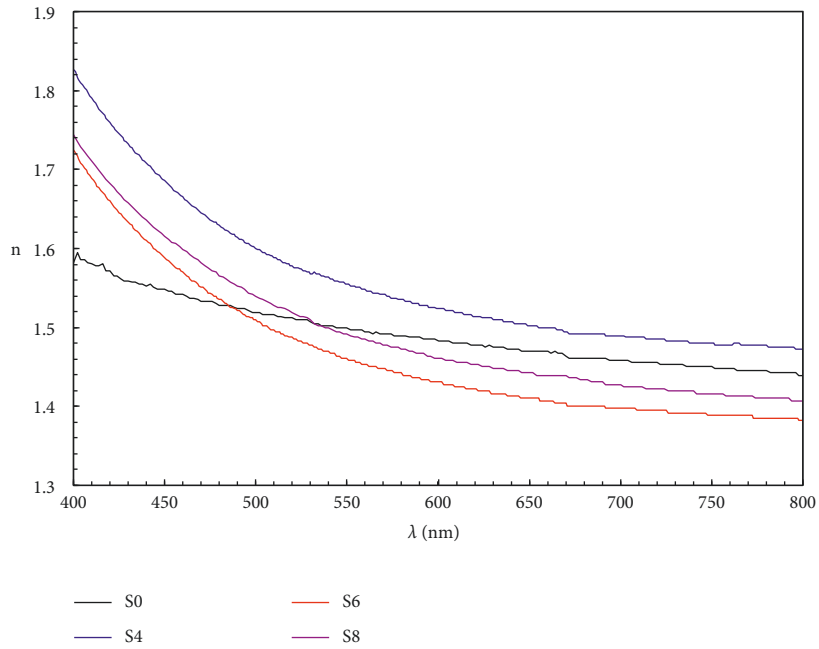

Figure 8: Variation of refractive index n with wavelength for CuONPs-doped HEC samples.

Table 3: Values of optical band gap (E_{opt}), number of carbon atoms (M) per carbonaceous cluster, and refractive index (n_o) for CuONPs-doped HEC samples.

Sample	E_{opt} (eV)	M	n_o
S0	5.40	~40	1.44
S4	5.10	~44	1.47
S6	5.30	~43	1.38
S8	5.20	~44	1.40

allowed, indirect forbidden, and indirect allowed, respectively.

The optical band gap E_{opt} values can be obtained by intercepting the linear fitted lines in the plots of $(\alpha h\nu)^2$ versus $h\nu$, as shown in Figure 7. Table 3 lists the determined optical band gap values. It was noted from Table 3 that the E_{opt} values reduce from 5.40 eV for the HEC sample to 5.10 eV for the S4 sample. For S6 and S8 samples, optical band gaps are 5.30 and 5.20 eV, respectively. The drop in the E_{opt} value might be assigned to the band formation between HEC polymer and CuO nanoparticles. Therefore, the lower energy transitions become possible because of the formation of trap levels between the HOMO and LUMO energy states which in turn lead to a decrease in the optical band gap [38]. Moreover, the optical band gap, E_{opt}, values can be associated with the number of carbon atoms per molecule through the expression [39]:

$$E_{opt} = \frac{34.3}{\sqrt{M}}, \tag{3}$$

where M is the carbon atoms number in the carbonaceous cluster. M values for copper oxide nanoparticles-doped hydroxyethyl cellulose films are calculated and listed in Table 3.

The calculated value of M for HEC was about 40, which could increase to 44 for other composite samples. This increase might be assigned to the conjugation increase in monomer units [39] in the matrix of HEC after loading CuONPs.

3.5.1. Refractive Index and Complex Dielectric Constant Analysis. The refractive index n, and extinction coefficient k, can be obtained by using the expression (4) that express the reflectivity of light on a material [40]:

$$R = \frac{\left[(n-1)^2 + k^2\right]}{\left[(n-1)^2 + k^2\right]}, \tag{4}$$

where n is the refractive index, $k = \alpha\lambda/4\pi$ is the extinction coefficient of material, and λ is incident photon wavelength. The refractive index is an important parameter in photoelectronic devices such as solar cell-related materials. Figure 8 shows the refractive index dispersion. It is noted that the refractive index drops when the wavelength of the incident photon increases and then reaches a constant value at longer wavelengths (n_0) as shown in Table 3. The decrease of refractive index with increasing wavelength proves the normal dispersion characteristics of samples due to the effectiveness of band levels. Reduction in polarizability, optical losses, and surface dispersion take place through normal dispersion because surface roughness and enhancement in carrier concentration are also reduced [41].

It is worth noting that the S4 sample has the largest refractive index for the overall wavelength range compared to other studied samples, and these variations of refractive index with wavelength enable HEC-CuONPs to be used in waveguide applications.

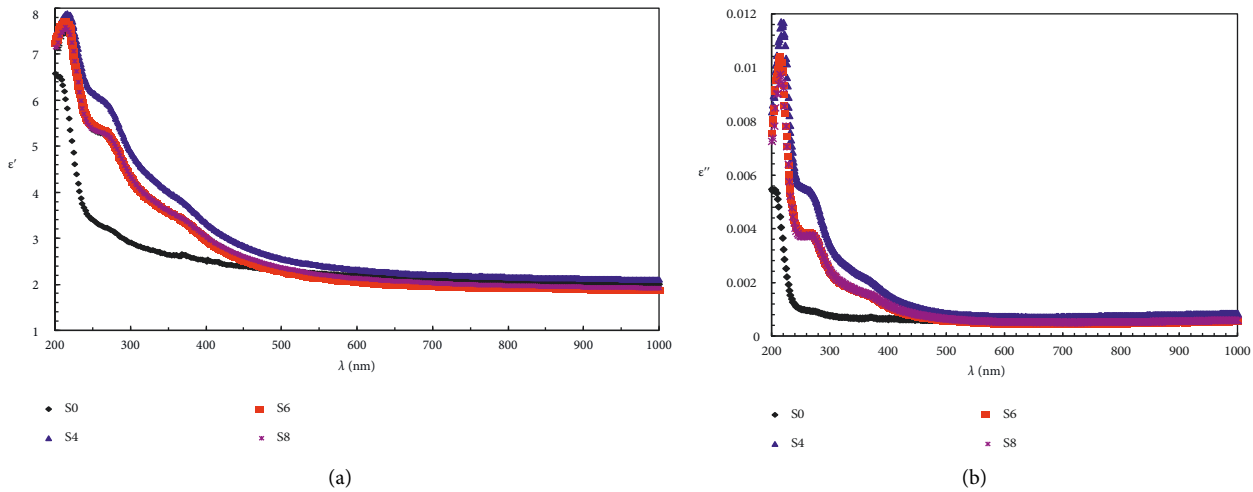

Figure 9: Plots of (a) dielectric constant ($\varepsilon\prime$) and (b) dielectric loss ($\varepsilon\prime\prime$) versus wavelength for CuONPs-doped HEC samples.

Expressions (5) and (6) were used to calculate the real and imaginary parts of the complex dielectric constant [42]:

$$\varepsilon\prime(\lambda) = n^2(\lambda) - k^2(\lambda), \tag{5}$$

$$\varepsilon\prime\prime(\lambda) = 2n(\lambda)k(\lambda), \tag{6}$$

where $\varepsilon\prime$ and $\varepsilon\prime\prime$ are calculated for CuONPs-HEC composite systems at different wavelengths. The dielectric components depend upon the polarizability of the sample, k, n values, and position density in the optical band gap [41]. As shown in Figures 9(a) and 9(b), there is a strong interaction between photons and electrons in the region from 200 to 600 nm. Also, $\varepsilon\prime$ and $\varepsilon\prime\prime$ decreased when the wavelength incident photon increases and they have peaks at certain energies (around optical energies). It is also noted that the S4 sample holds the largest $\varepsilon\prime$ and $\varepsilon\prime\prime$ over the whole wavelength range.

4. Conclusions

Copper oxide nanoparticles were prepared successfully by the chemical reduction method. The formation of CuONPs was confirmed by X-ray, UV-vis, and TEM results. The optical properties of hydroxyethyl cellulose (HEC) were effectively enhanced by adding CuONPs but no significant effect was observed on the thermal stability of CuONPs-HEC composites. The enhancement of the optical properties of HEC loaded with CuONPs opens the doors for many potential applications [18].

Data Availability

The data that support the findings of this study are available from the corresponding author upon reasonable request.

Conflicts of Interest

The authors declare that they have no known competing financial interests or personal relationships that could have appeared to influence the work reported in this paper.

Acknowledgments

The authors would like to acknowledge the financial support of the Taif University Researchers Supporting Project number (TURSP-2020/189), Taif University, Taif, Saudi Arabia.

References

[1] B. Zhao, X. Lu, Q. Wang, J. Yang, J. Zhao, and H. Zhou, "Salt-triggered Active Plasmonic Systems Based on the Assembly/Disassembly of Gold Nanorods in a DNA Brush Layer on a Solid Substrate," *Chinese Chemical Letters*, vol. 31, p. 831, 2020.

[2] H. B. Mikhail, M. M. Nagy, S. Emam, K. S. Nagy, and H. E. Emam, "pH responsive intelligent nano-engineer of nanostructures applicable for discoloration of reactive dyes," *Journal of Colloid and Interface Science*, vol. 561, pp. 147–161, 2020.

[3] E. C. Dreaden, A. M. Alkilany, X. Huang, C. J. Murphy, and M. A. El-Sayed, "The golden age: gold nanoparticles for biomedicine," *Chemical Society Reviews*, vol. 41, no. 7, pp. 2740–2779, 2012.

[4] L. M. Liz-Marzán, "Nanometals: Formation and color," *Materials Today*, vol. 7, pp. 26–31, 2004.

[5] H. B. Ahmed, A. M. Abdel-Mohsen, and H. E. Emam, "Green-assisted tool for nanogold synthesis based on alginate as a biological macromolecule," *RSC Advances*, vol. 6, no. 78, pp. 73974–73985, 2016.

[6] K. H. Mahmoud, "Synthesis, characterization, optical and antimicrobial studies of polyvinyl alcohol-silver nano-composites," *Spectrochimica Acta Part A: Molecular and Biomolecular Spectroscopy*, vol. 138, p. 434, 2015.

[7] Z. Tang, N. A. Kotov, S. Magonov, and B. Ozturk, "Nano-structured artificial nacre," *Nature Materials*, vol. 2, no. 6, pp. 413–418, 2003.

[8] J. J. Schneider, "Magnetic core/shell and quantum-confined semiconductor nanoparticles via chimie douce organometallic synthesis," *Advanced Materials*, vol. 13, no. 7, pp. 529–533, 2001.

[9] K. Misiakos, S. E. Kakabakos, P. S. Petrou, and H. H. Ruf, "A monolithic silicon optoelectronic transducer as a real-time

affinity biosensor," *Analytical Chemistry*, vol. 76, no. 5, pp. 1366–1373, 2004.

[10] M. Mobin and M. Rizvi, "Adsorption and corrosion inhibition behavior of hydroxyethyl cellulose and synergistic surfactants additives for carbon steel in 1 M HCl," *Carbohydrate Polymers*, vol. 156, pp. 202–214, 2017.

[11] Q. Zhang, K. Xu, S Yang et al., "CuO nanostructures: synthesis, characterization, growth mechanisms, fundamental properties, and applications," *Progress in Materials Science*, vol. 60, pp. 208–337, 2014.

[12] J. F. Xu, W. Ji, Z. X. Shen et al., "Preparation and characterization of CuO nanocrystals," *Journal of Solid State Chemistry*, vol. 147, no. 2, pp. 516–519, 1999.

[13] K. Kwak and C. Kim, "Korea–Australia," *Rheol J*, vol. 17, p. 35, 2005.

[14] A. Waris, M. Din, A. Ali et al., "A comprehensive review of green synthesis of copper oxide nanoparticles and their diverse biomedical applications," *Inorganic Chemistry Communications*, vol. 123, Article ID 108369, 2021.

[15] H. E. Attia, M. A. El-Dars, F. M. S. E. Ahmed, and H. B. Ahmed, "Emerging use of homogenic and heterogenic nano-colloids synthesized via size-controllable technique in catalytic potency," *Journal of Polymers and the Environment*, vol. 28, no. 2, pp. 553–565, 2020.

[16] H. E. Mikhail, M. M. Nagy, S. Ahmed, K. S. Nagy, and H. B. Ahmed, "Metal-dependent nano-catalysis in reduction of aromatic pollutants," *Environmental Science and Pollution Research*, vol. 27, no. 6, pp. 6459–6475, 2020.

[17] H. B. Ahmed and H. E. Emam, "Seeded growth core-shell (Ag–Au–Pd) ternary nanostructure at room temperature for potential water treatment," *Polymer Testing*, vol. 89, Article ID 106720, 2020.

[18] S. Panigrah, S. Kundu, S. K. Ghosh, S. Nath, B. Soumen, and T. Pal, "Selective one-pot synthesis of copper nanorods under surfactantless condition," *Polyhydron*, vol. 25, p. 1263, 2006.

[19] A. Y. Booshehri, R. Wang b, and R. Xu, "Supports open access," *Chemical Engineering Journal*, vol. 262, p. 999, 2015.

[20] S. Panigrah, S. Kundu, S. K. Ghosh, S. Nath, and T. Pal, "General method of synthesis for metal nanoparticles," *Journal of Nanoparticle Research*, vol. 6, p. 411, 2004.

[21] R. Seoudi, A. B. El- Bailly, W. Eisa et al., "Synthesis, optical and dielectric properties of (PVA/CdS) nanocomposites," *Journal of Applied Sciences Research*, vol. 8, p. 658, 2012.

[22] G. Ren, D. Hu, E. W. C. Cheng, M. A. Vargas-Reus, P. Reip, and R. P. Allaker, "Characterisation of copper oxide nanoparticles for antimicrobial applications," *International Journal of Antimicrobial Agents*, vol. 33, no. 6, pp. 587–590, 2009.

[23] A. A. Hassabo, E. I. Ibrahim, B. A. Ali, and H. E. Emam, "Anticancer effects of biosynthesized Cu2O nanoparticles using marine yeast," *Biocatalysis and Agricultural Biotechnology*, vol. 39, Article ID 102261, 2022.

[24] K. A. Bogle, S. D. Dhole, and V. N. Bhoraskar, "Silver nanoparticles: synthesis and size control by electron irradiation," *Nanotechnology*, vol. 17, no. 13, pp. 3204–3208, 2006.

[25] O. Alekseeva, S. Chulovskaya, N. Bagrovskaya, and V. Parfenyuk, "Copper nanopartical composites based on cellulose derivatives," *Chemistry & Chemical Technology*, vol. 5, no. 4, pp. 447–450, 2011.

[26] R. Chen, C. Yi, H. Wu, and S. Guo, "Degradation kinetics and molecular structure development of hydroxyethyl cellulose under the solid state mechanochemical treatment," *Carbohydrate Polymers*, vol. 81, no. 2, pp. 188–195, 2010.

[27] T. Gong, Y. Hou, X. Yang, and Y. Guo, "Gelation of hydroxyethyl cellulose aqueous solution induced by addition of colloidal silica nanoparticles," *International Journal of Biological Macromolecules*, vol. 134, pp. 547–556, 2019.

[28] G. Attia and M. F. H. Abd El-kader, "Structural, Optical and Thermal Characterization of PVA/2HEC Polyblend Films," *International Journal of Electrochemical Science*, vol. 8, p. 5672, 2013.

[29] S. C. Angadi, L. S. Manjeshwar, and T. M. Aminabhavi, "Interpenetrating polymer network blend microspheres of chitosan and hydroxyethyl cellulose for controlled release of isoniazid," *International Journal of Biological Macromolecules*, vol. 47, no. 2, pp. 171–179, 2010.

[30] P. Budrugeac, "Kinetics of the complex process of thermo-oxidative degradation of poly(vinyl alcohol)," *Journal of Thermal Analysis and Calorimetry*, vol. 92, no. 1, pp. 291–296, 2008.

[31] S. Rajendran, M. Sivakumar, R. Subadevi, and M. Nirmala, "Characterization of PVA-PVdF based solid polymer blend electrolytes," *Physica B: Condensed Matter*, vol. 348, no. 1–4, pp. 73–78, 2004.

[32] R. Anbarasan, R. Pandiarajaguru, R. Prabhu et al., "Synthesis, characterizations, and mechanical properties of structurally modified poly(vinyl alcohol)," *Journal of Applied Polymer Science*, vol. 117, no. 4, pp. 2059–2068, 2010.

[33] Z. Peng and L. X. Kong, "A thermal degradation mechanism of polyvinyl alcohol/silica nanocomposites," *Polymer Degradation and Stability*, vol. 92, no. 6, pp. 1061–1071, 2007.

[34] K. H. Mahmoud, A. SA. Elsayed, and K. A. Elsayed, "Modulation of optical properties of PolyvinylPyrrolidone via doping with praseodymium (III) nitrate salt," *Optik*, vol. 231, Article ID 166383, 2021.

[35] M. A. Morsi and A. M. Abdelghany, "UV-irradiation assisted control of the structural, optical and thermal properties of PEO/PVP blended gold nanoparticles," *Materials Chemistry and Physics*, vol. 201, pp. 100–112, 2017.

[36] R. Rawat, A. Tiwari, N. Arun, S. V. S. N. Rao, A. P. Pathak, and A. Tripathi, "Solvents effect on the morphology and stability of Cu/CuO nanoparticles synthesized at high fluence laser ablation," *ChemistrySelect*, vol. 4, no. 35, pp. 10471–10482, 2019.

[37] R. Vahalová, L. Tichý, M. Vlček, and H. Tichá, "Far infrared spectra and bonding arrangement in some ge–sb–s glasses," *Physica Status Solidi A*, vol. 181, p. 199, 2000.

[38] R. P. Chahal, S. Mahendiu, A. K. Tomar, and S. Kumar, "Effect of ultraviolet irradiation on the optical and structural characteristics of in-situ prepared pvp-ag nanocomposites," *Dig. J. Nanomater. Bios*, vol. 6, p. 299, 2011.

[39] D. Fink, W. H. Chung, R. Klett et al., "Carbonaceous clusters in irradiated polymers as revealed by UV-Vis spectrometry," *Radiation Effects and Defects in Solids*, vol. 133, p. 193, 1995.

[40] D. P. Gosain, T. Shimizu, M. Ohmura, M. Suzuki, T. Bando, and S. Okano, "Some properties of Sb2Te3–xSex for non-volatile memory based on phase transition," *Journal of Materials Science*, vol. 26, no. 12, pp. 3271–3274, 1991.

[41] C. Ayden, "Supports open access," *J.Alloys and Compounds*, vol. 777, 2019.

[42] A. A. Al-Ghamdi, "Optical band gap and optical constants in amorphous Se96–xTe4Agx thin films," *Vacuum*, vol. 80, no. 5, pp. 400–405, 2006.